ADVANCED FUNCTIONAL MATERIALS
www.afm-journal.de

Laminated Perovskite Photovoltaics: Enabling Novel Layer Combinations and Device Architectures

*Raphael Schmager, Julie Roger, Jonas A. Schwenzer, Fabian Schackmar, Tobias Abzieher, Mahdi Malekshahi Byranvand, Bahram Abdollahi Nejand, Matthias Worgull, Bryce S. Richards, and Ulrich W. Paetzold**

High-efficiency perovskite-based solar cells can be fabricated via either solution-processing or vacuum-based thin-film deposition. However, both approaches limit the choice of materials and the accessible device architectures, due to solvent incompatibilities or possible layer damage by vacuum techniques. To overcome these limitations, the lamination of two independently processed half-stacks of the perovskite solar cell is presented in this work. By laminating the two half-stacks at an elevated temperature (≈90 °C) and pressure (≈50 MPa), the polycrystalline perovskite thin-film recrystallizes and the perovskite/charge transport layer (CTL) interface forms an intimate electrical contact. The laminated perovskite solar cells with tin oxide and nickel oxide as CTLs exhibit power conversion efficiencies of up to 14.6%. Moreover, they demonstrate long-term and high-temperature stability at temperatures of up to 80 °C. This freedom of design is expected to access both novel device architectures and pairs of CTLs that remain usually inaccessible.

1. Introduction

Extensive research on perovskite-based photovoltaics (PV) over the past decade led to rapid development, with power conversion efficiencies (PCEs) exceeding 25.2% being realized.[1] Hybrid organic–inorganic metal halide perovskite semiconductors continue to attract enormous attention due to their exceptional optoelectronic properties, such as their high absorption coefficients, high carrier mobilities, and low recombination rates.[2,3] The widely tunable bandgap of these perovskites by compositional variations of the halide anion in the perovskite crystal structure allows strong light absorption in a broad spectral range.[4] With their low material costs and a wide range of possible deposition techniques,[5] perovskites qualify as promising candidates for next-generation multi-junction PV.[6,7] Moreover, combined with established PV technologies, like wafer-based silicon or copper indium gallium selenide films, perovskite-based tandems are currently the most promising technology for terrestrial PV to enable PCEs exceeding the single-junction Shockley–Queisser limit.[8]

The recent development in perovskite PV has been largely underpinned by advances in the composition[9,10] and morphology[11] of the perovskite absorber layer as well as progress in device architectures[12] by employing passivation layers[13,14] and optimizing hole and electron transport layers (HTLs and ETLs).[15,16] Nevertheless, fundamental challenges, such as the toxicity of lead-based perovskites, the limited stabilities of the various layers—such as the perovskite absorber, charge transport layers (CTL), and combinations thereof—in terms of moisture, light, and heat stress remain to be solved. One promising route to cope the stability of the devices is via the replacement of organic CTLs with inorganic counterparts. In this regard, the HTLs, copper iodide (CuI), copper thiocyanate (CuSNC), and nickel oxide (NiO_x) have been shown to promise good intrinsic chemical stability compared to the commonly used organic HTL spiro-OMeTAD.[15,17–19] In addition, ETLs like zinc oxide (ZnO), tin oxide (SnO_2), and mesoporous titanium dioxide (TiO_2) are known to be intrinsically stable and have been demonstrated to result in highly efficient and stable perovskite solar cells.[20–24]

However, conventional methods for layer deposition significantly limits the choice of materials, deposition techniques, and device architectures, due to solvent incompatibilities or process-induced damage of underlying layers during vacuum-based physical vapor deposition (PVD) and chemical vapor deposition (CVD) processes.[25–27] Whereas the CTL under the perovskite must be robust against the perovskite deposition, many polar solvents have to be avoided for the layers, which are solution-processed on top of the perovskite to prevent decomposition or degradation. Similarly, high temperatures, radicals, and ion

R. Schmager, J. Roger, Dr. M. Malekshahi Byranvand, Dr. B. Abdollahi Nejand, Dr. M. Worgull, Prof. B. S. Richards, Dr. U. W. Paetzold
Institute of Microstructure Technology
Karlsruhe Institute of Technology (KIT)
Hermann-von-Helmholtz-Platz 1, 76344 Karlsruhe, Germany
E-mail: ulrich.paetzold@kit.edu

J. A. Schwenzer, F. Schackmar, Dr. T. Abzieher, Prof. B. S. Richards, Dr. U. W. Paetzold
Light Technology Institute
Karlsruhe Institute of Technology (KIT)
Engesserstrasse 13, 76131 Karlsruhe, Germany

The ORCID identification number(s) for the author(s) of this article can be found under https://doi.org/10.1002/adfm.201907481.

DOI: 10.1002/adfm.201907481

bombardment must be limited due to the possible damage of the underlying layers during PVD and CVD techniques such as sputtering, atomic layer deposition, or electron-beam evaporation. In this regard, metal-oxide or fullerene-based buffer layers are usually employed that protect the underlying absorber layer.[28–31] Therefore, not every combination of ETL and HTL is accessible in a straightforward manner.

In order to circumvent these challenges, lamination of different electrodes and mesh-like CTLs on the perovskite layer have been suggested in the literature.[32–35] Moreover, the lamination with wet organic CTLs has been presented in tandem[36,37] and semitransparent flexible perovskite solar cells.[38] In addition, the lamination of dry organic layers on top of each other[39–41] and directly on the perovskite absorber has been introduced.[42] Recently, Dunfield et al. presented a first proof-of-concept of the pressure-assisted lamination of two perovskite layers on top of each other, which is a promising technique suitable for industrial large-scale roll-to-roll fabrications.[43] However, so far, the PCE remains comparably low (<11%) and in particular, no stable power outputs have been demonstrated. Nevertheless, according to Shi et al. and Kim et al. the pressure applied to the perovskite layer during a hot-pressing process, which is similar to the lamination process, can be beneficial for the device performance.[44,45]

In this work, we report on our recent progress on laminated perovskite solar cells using a hot pressing process at significantly lower temperatures than reported previously. This advance enables highest PCEs of up to 14.6% for laminated perovskite solar cells and, most importantly, leads to a stable power output. The laminated perovskite solar cells demonstrate long-term stable PCEs and excellent thermal stability for temperatures of up to 80 °C. In this study, we report on the fabrication method of laminated perovskite solar cells via a facile hot pressing process. Furthermore, the recrystallization of the perovskite layer and lamination onto the HTL and ETL interface is analyzed in detail. In addition, the use of a thin poly(triarylamine) (PTAA) polymer buffer layer between the HTL/perovskite interface is shown to improve the mechanical and electrical contact. The presented lamination method opens up the possibility to access new device architectures and material combinations that are difficult or even impossible to process by conventional methods. Additionally, the lamination of the perovskite is a promising tool for novel tandem designs, enabling new architectures and direct encapsulation of the solar modules. To confirm the versatility of the proposed lamination method in prospect of future tandem applications, we further demonstrate laminated semitransparent and laminated flexible perovskite solar cells.

2. Results and Discussion

The lamination of perovskite solar cells is a promising strategy to enable device architectures and material combinations in perovskite PV, which are inaccessible by conventional processing methods. In order to demonstrate the potential of this method, devices featuring oxide CTLs (SnO_2 and sputtered NiO_x) are processed. Additionally, the influence of a thin PTAA polymer buffer layer in between the perovskite and HTL is discussed. The laminated perovskites solar cells are produced via hot pressing of two independently fabricated half-stacks (see **Figure 1**). In this regard, the front half-stack (A) of the perovskite solar cell is processed on top of a glass substrate and the rear half-stack (B) of the perovskite solar cell is processed on top of a flexible polyethylene naphthalate (PEN) foil. The perovskite absorber is brought into contact with the HTL and subsequently laminated together. A triple-cation perovskite $Cs_{0.1}(MA_{0.17}FA_{0.83})_{0.9}Pb(I_{0.83}Br_{0.17})_3$ thin-film serves as the absorber. For more details on the layer preparation, see the Experimental Section. The two half-stacks of the perovskite solar cell are laminated at a temperature of 90 °C and a pressure of ≈50 MPa via a hot pressing method. The corresponding process diagram is displayed in Figure S1 in the Supporting Information. The heating and cooling of the sample is achieved by controlling the temperature of the upper and lower plate of the hot pressing machine (see Figure 1). The process pressure is kept constant for 5 min once the lamination temperature is reached. After 5 min, a cool down of the laminated perovskite

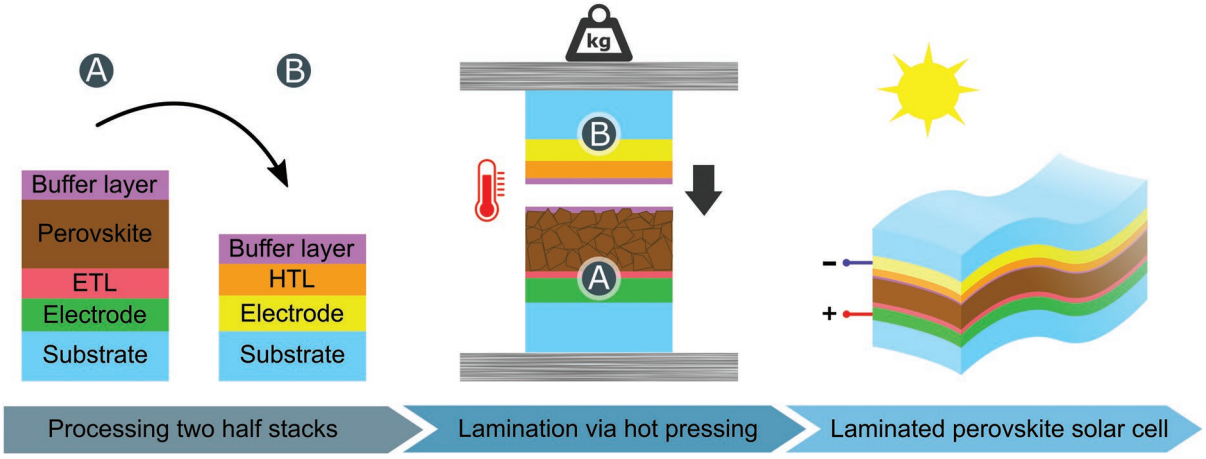

Figure 1. Schematic illustration of the lamination process of perovskite solar cells. Two separate half-stacks are fabricated and subsequently laminated in a hot-pressing step. The hot pressing is performed in nitrogen atmosphere at 90 °C and a pressure of ≈50 MPa. The pressure is kept constant at the lamination temperature for 5 min. The pressure is released once the sample is cooled down to room temperature. With the lamination, homogenous perovskite solar cells are produced.

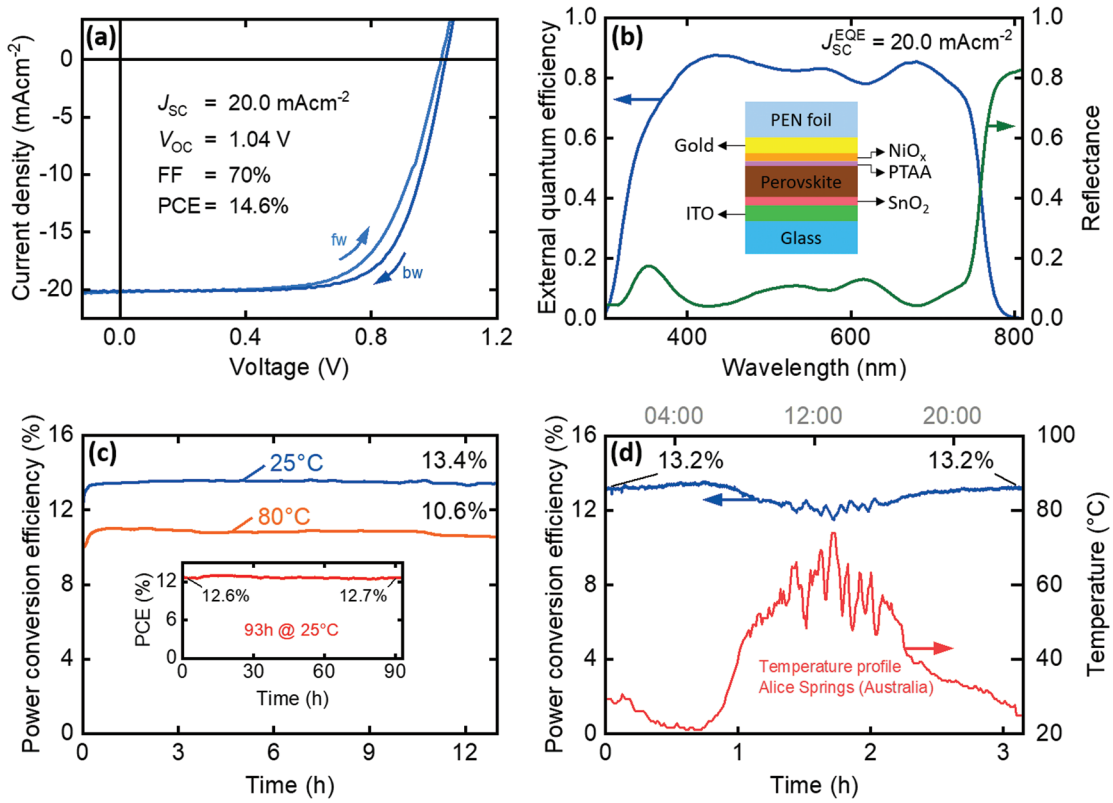

Figure 2. a) Current density–voltage characteristics and b) the EQE and the corresponding reflectance of the champion laminated perovskite solar cell. The inset shows the device architecture. c) Stabilized MPP tracking for 25 and 80 °C. d) MPP tracking with a measured outdoor temperature profile of a silicon module at the hottest day in Alice Springs (Australia) in 2014 (measured by the Desert Knowledge Australia Solar Center).

solar cell is initialized and the pressure is held constant until the sample reaches 40 °C.

Making use of the new fabrication route, we process laminated perovskite solar cells that exhibit high stability and remarkable PCEs. The current density–voltage characteristics (*J*–*V*) of the laminated champion perovskite solar cell is displayed in **Figure 2**a. The device shows a PCE of 14.6%, which is 38%$_{rel}$ (or 4%$_{abs}$) higher in PCE than the reported value for a comparable laminated device architecture using $MAPbI_3$ (methylammonium lead triiodide) perovskite instead of the triple-cation perovskite as absorber material.[43] The champion device exhibits a short-circuit current density (J_{SC}) of 20.0 mA cm^{-2} (see Figure 2b and Table S1, Supporting Information), an open-circuit voltage (V_{OC}) of 1.04 V, and a fill factor (FF) of 70%. Moreover, for the first time, the devices demonstrate a stable power output (see Figure S2, Supporting Information), which is the key for evaluating a realistic power output given the uncertainties that arise from hysteresis effects in perovskite PV. The PCE under maximum power point (MPP) tracking over 13 h at 25 and at 80 °C are displayed in Figure 2c. The champion laminated perovskite solar cell shows a stabilized PCE (SPCE) at 25 and 80 °C of 13.4% and 10.6%, respectively. Even after 93 h of MPP tracking, the device still exhibited a stable power output (see inset Figure 2c). This very remarkable stability against light and temperature stress is founded in the use of inorganic CTLs and particularly the replacement of the organic CTLs like spiro-OMeTAD which is known to degrade at elevated temperatures > 60 °C.[15,46–48]

Since temperature variations are inevitable in outdoor device operations and might have a detrimental effect on the power output over time,[49] the laminated perovskite solar cells are also stressed with an outdoor temperature profile (see Figure 2d).[50] The module temperature is measured in Alice Springs (Australia) and the temperatures are ranging from 20 to 75 °C (for details on the measured temperature profile see ref. [50]). In order to accelerate the temperature variations, the 24 h temperature profile of the hottest day in the dataset is compressed to ≈3 h. The laminated perovskite solar cells confirm a high stability, manifested in the almost identical PCE of 13.2% before and after the realistic temperature profile. Compared to a similar architecture with spiro-OMeTAD, the laminated perovskite solar cells with NiO_x as HTL appear more stable against temperature variations.[49] The stabilities under constant thermal stress, temperature variations, and long-term MPP tracking, are an important step toward stable perovskite PV. The laminated perovskite solar cells do not show any decrease in the initial PCE after 93 h of MPP tracking, which is equally good to current carbon-based perovskite solar cells, known for their superior stabilities.[51,52] Therefore, the constant power output of laminated perovskite solar cells is remarkable given the previously reported reversible loss up to 10% in the first ≈100 h of triple-cation perovskite solar cells in an *n-i-p* configuration.[53,54] In addition to that, the decrease in initial PCE of only ≈4% at elevated temperatures is comparable to carbon-based perovskite solar cells.[55,56] However, the laminated perovskite solar cells still have to compete with currently reported stabilities over

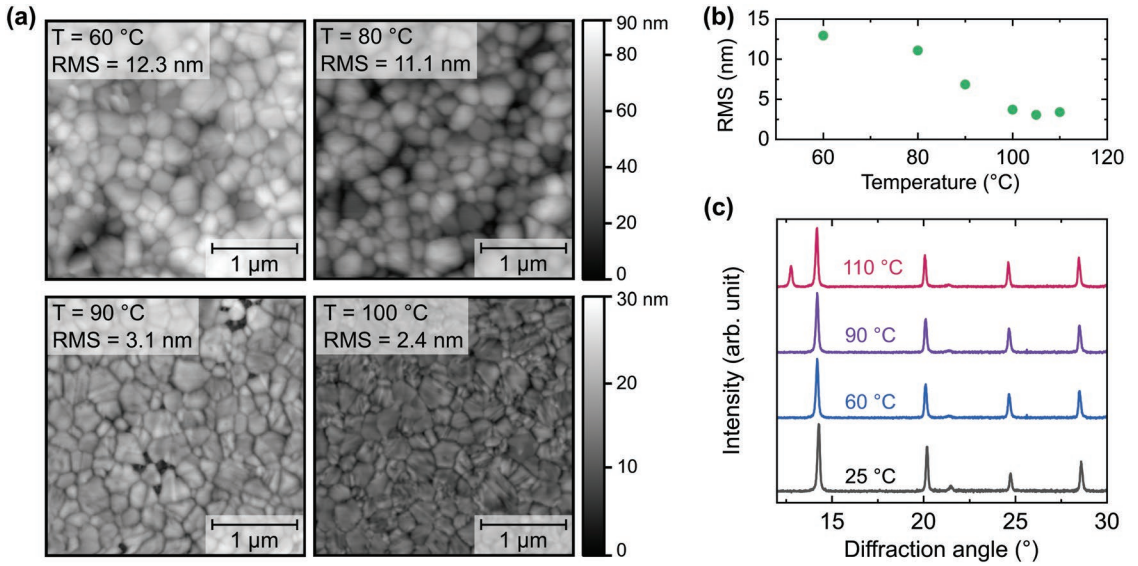

Figure 3. a) AFM images of delaminated perovskite surfaces. The delamination is performed at the perovskite/NiO_x interface (without any PTAA buffer layer) after the devices have been laminated at 60, 80, 90, and 100 °C. The architecture is glass/ITO/SnO_2/perovskite. b) The RMS roughness of the perovskite surface decreases with the lamination temperature. c) XRD pattern of the triple-cation perovskite at increasing temperatures indicates no decomposition or degradation for lamination temperatures of up to 90 °C.

1000 h.[55,57,58] We hypothesize that the stability of the laminated perovskite solar cells is afforded via the replacement of the organic spiro-OMeTAD as HTL. Moreover, via the lamination of the two half-stacks of the perovskite solar cell, the devices are encapsulated by the two substrates, providing potential barrier properties against oxygen and moisture.[59] From a technological perspective, this is very appealing, since it might combine fabrication and encapsulation to a one-step self-encapsulation process without the need for an external adhesive.

Key to the lamination process introduced in this study is a thin PTAA buffer layer at the perovskite/NiO_x interface. For the champion devices, the two top layers (perovskite and NiO_x), which are usually exposed to ambient atmosphere during the hot pressing, are covered with a thin buffer layer of PTAA (see the Experimental Section for details) during the preparation of the two-half-stacks. Compared to the laminated perovskite solar cells processed without the PTAA buffer layer, the mean device performance is enhanced by 6.9%$_{abs}$ (see also Figure S3, Supporting Information). The PTAA layer enhances the mechanical and electrical contact of the laminated perovskite solar cells. The improved mechanical contact between the laminated layers can be seen by 36% less nonfunctional laminated perovskite solar cells (see Figure S4, Supporting Information). Furthermore, it is hypothesized that the PTAA layer is able to fill remaining holes in between the recrystallized perovskite layer (see **Figure 3**a) and the NiO_x HTL. Since the glass transition temperature of the PTAA is > 100 °C,[60] this allows to maintain good thermal stability. Compared to the laminated perovskite solar cells without the buffer layer, the devices demonstrate an increased FF (see Figures S3 and S5, Supporting Information), which is directly related to an improved shunt and series resistance. Compared to the devices without the PTAA buffer layer, the series resistance in the champion laminated perovskite solar cells reduces from ≈180 to ≈60 Ω. Moreover, the shunt resistance of the champion laminated perovskite solar cell drastically improved compared to the previous report (see ref. [43]). Nevertheless, the electrical parameters lack still behind record perovskite solar cells, with optimized architectures. However, the lamination of the two individually processed half-stacks provides the possibility to implement new materials and to access new device architectures. To further increase the electrical parameters of the laminated perovskite solar cells, additional optimizations of the process parameters are needed.

From a process perspective, the lamination of the perovskite layer on top of the NiO_x HTL is strongly dependent on the lamination temperature. At higher lamination temperature, the FF of the solar cells is increased (see Figure S6, Supporting Information). To analyze the perovskite recrystallization during the lamination, atomic force microscopy (AFM) images of delaminated perovskite solar cells—previously processed by the lamination method—are analyzed (see Figure 3a). For rising lamination temperatures, the roughness of the layer is decreasing. The average roughness of the AFM scans is displayed in Figure 3b. The optimum in device performance is found at 90 °C, which is in line with temperatures used for nanoimprinted perovskite layers.[61–65] Here, the perovskite recrystallizes to very smooth layers with root mean square (RMS) roughness around 3.1 nm (see Figure 3a,b). Further increase in the lamination temperature reduces the RMS roughness additionally but does not lead to higher PCEs (see Figure S5, Supporting Information). Even though the transfer of the sample into the hot-pressing machine is conducted in ambient atmosphere, and the laminated perovskite layer is subjected to high pressures and elevated temperatures, the crystal structure of the triple-cation perovskite remains unaltered (see Figure 3c). In the X-ray diffraction (XRD) pattern, the characteristic diffraction peaks from the crystal planes of the triple-cation perovskite (half-stack) are evident and no degradation is visible for lamination

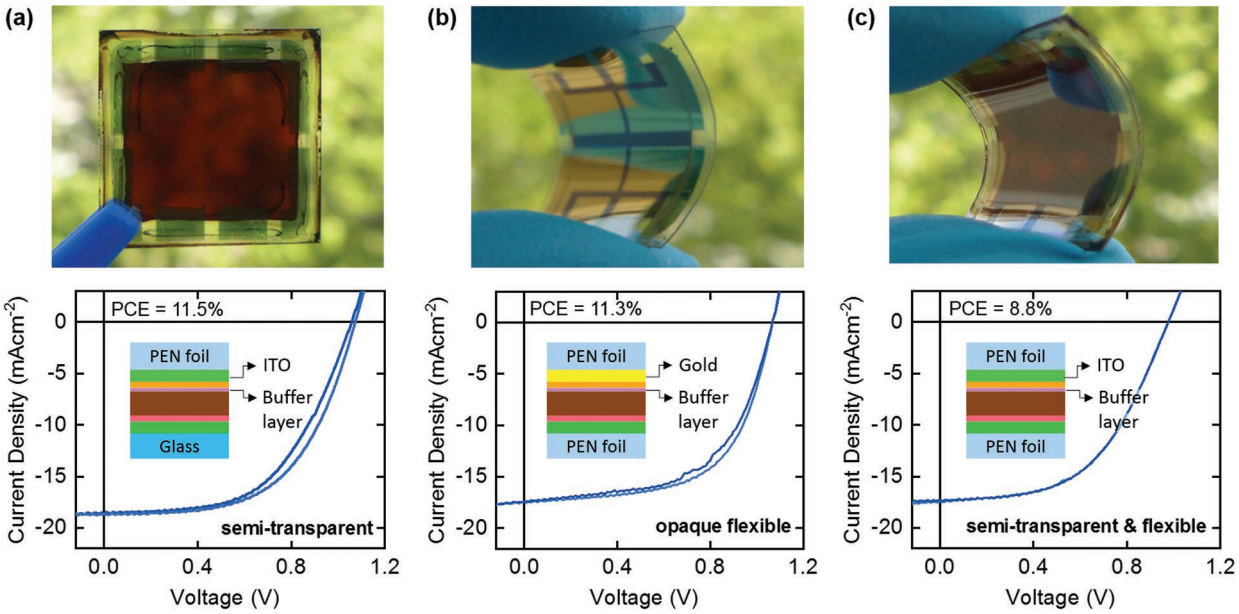

Figure 4. Current density–voltage characteristics and corresponding photographs of a) a rigid semi-transparent, b) an opaque and flexible, and c) a semi-transparent and flexible laminated perovskite solar cell. Except of the different electrodes and substrates, the laminated solar cells are made of the same architecture: substrate/ITO/SnO_2/perovskite/buffer layer/NiO_x/electrode/substrate.

temperatures up to 90 °C. Only for temperatures above 110 °C, a significant PbI_2 diffraction peak is noticeable.

With view on the technology's perspective, laminated perovskite solar cells presented in this work provide several degrees of freedom to the processing routes of thermal evaporation and liquid processing. This freedom encompasses new material combinations and device architectures. To demonstrate the versatility of the lamination, a) semitransparent, b) flexible opaque, and c) flexible semitransparent perovskite solar cells are processed (see **Figure 4**). In the semitransparent devices, a 150 nm thick sputtered indium-doped tin oxide (ITO) layer replaces the gold electrode. The laminated semitransparent solar cell shows a PCE of 11.5% (SPCE of 11.4%). For the flexible perovskite solar cells, a second flexible PEN foil replaces the rigid glass. By laminating the two half-stacks processed on the PEN substrates, the flexible opaque perovskite solar cell demonstrates a PCE of 11.3% (SPCE of 11.2%). By replacing the gold with an ITO electrode, the laminated semitransparent device achieves a PCE of 8.8%.

Compared to previous literature,[43] the PCE of the presented laminated perovskite solar cells represent a significant advance. The novel lamination strategy, using a thin PTAA buffer layer together with the NiO_x HTL, improves the PCE from 10.6%[43] to 14.6%. However, in comparison to record cesium-containing triple-cation perovskite solar cells,[66–68] the PCEs are still far behind. In particular, the V_{OC} of only ≈1.04 V and the FF of 70% are not yet optimal and lack ≈15–20% behind the record perovskite solar cells processed by spin coating. This we attribute to remaining losses by the series resistance and imperfect interfaces. Future work will have to address these aspects by interfacial engineering, passivation layers, or improving the band energy alignment. In addition, the J_{SC} of the laminated perovskite solar cells are around 10% lower than the record perovskite solar cells with a similar bandgap. This can be addressed by improvements in the transmittance of the front ITO contact and the deployment of an antireflection coating at the front air/glass interface. However, the presented lamination process leads to stable power outputs, which are encouraging for future research on laminated perovskite PV. The approach offers versatility that can be exploited to optimize the architecture and employed materials with regard to stability. This is one of the major concerns these days of perovskite PV. Particularly, the presented lamination of the perovskite solar cells offers a promising route to access all-inorganic architectures. Moreover, the lamination enables further investigations on inverted architectures, avoiding TiO_2 as front CTL, to enhance robustness against UV light-induced degradation.[69]

In addition, combining different optical and electronic characteristics of distinct perovskite materials might be beneficial for boosting the overall device performance. However, the combination of various perovskite compositions in a single device is challenging, since sufficient selectivity of the used solvents for different perovskite materials is needed. To resolve this issue, Wang et al. recently reported on a two-step solution-based approach, where a micro-crystalline $MAPbI_3$ film is processed on top of a nano-crystalline perovskite $MAPbI_3$ film.[70] Cui et al. demonstrated a perovskite–perovskite homojunction by thermally evaporating a p-type perovskite layer (MA-rich) on top of a solution-processed n-type perovskite layer (Pb-rich), efficiently reducing carrier recombination losses in the devices.[71] However, further combinations (e.g., different bandgaps) would be very interesting to investigate. In this regard, the presented lamination process offers another valuable possibility to explore further combinations of multilayer perovskite thin films by facile lamination of the distinct perovskite layers via a hot pressing process.

From the authors' perspective, future application of laminated perovskite solar cells in perovskite-based tandem PV is very exciting as well, as it offers a promising route to enable

roll-to-roll processing with the potential of direct encapsulation of the modules. For perovskite-based tandem solar modules, the top perovskite half-stack could be prepared separately and subsequently laminated on top of the bottom solar cell to form a two-terminal tandem module.

3. Conclusion

In this work, we report on a facile route to fabricate perovskite solar cells via the lamination of two separately processed half-stacks. This enables access to novel device architectures and brings further degrees of freedom in the choice of the ETL and the HTL. We present the lamination of the perovskite solar cells at the HTL/perovskite interface with PCEs of up to 14.6%. We demonstrate for the first time the long-term and high-temperature stability for the laminated perovskite solar cells equipped with two inorganic CTLs. The champion device shows a stable power output (≈12.7%) after almost 100 h of MPP tracking and high-temperature stability for temperatures of up to 80 °C. The devices recover to its initial PCEs during MPP tracking, even after heating with realistic module temperatures. Moreover, we demonstrate flexible and semitransparent laminated perovskite solar cells in perspective to future tandem applications. In this regard, the presented lamination method will be useful to create self-encapsulated architectures or even multi-junction perovskite-based solar modules. In case of multi-junction PV, the half-stack with the perovskite absorber could be laminated directly on top of a bottom solar cell to build a two-terminal tandem solar cell.

4. Experimental Section

Device Preparation: Prepatterned ITO substrates on glass (Luminescence Technology) and on PEN foil (Diamond Coatings) were cleaned in ultrasonic baths of detergent, deionized water, acetone, and isopropyl alcohol for 10 min each. The glass and flexible foil substrates were 16 mm × 16 mm. A 15% aqueous colloidal dispersion of tin oxide (SnO_2) (Alfa Aesar) was diluted to a final concentration of 2%. Subsequently, the SnO_2 ETL was spin-coated at a speed of 4000 rpm for 30 s. The spin-coated SnO_2 layer was then annealed in air at 250 °C (for the glass substrates) and 110 °C (for the foil substrates) for 30 min.

The triple-cation perovskite absorber solution $Cs_{0.1}(MA_{0.17}FA_{0.83})_{0.9}Pb(I_{0.83}Br_{0.17})_3$ was prepared according to ref. [24] with the precursors of methylammonium bromide (MABr, GreatCell Solar), formamidinium iodide (FAI, GreatCell Solar), lead iodide (PbI_2, TCI), lead bromide ($PbBr_2$, TCI), and cesium iodide (CsI, Alfa Aesar). Two solutions were prepared: 1) CsI in dimethyl sulfoxide (DMSO; 1.5 M, Sigma Aldrich) and 2) FAI (1 M), PbI_2 (1.1 M), MABr (0.2 M), and $PbBr_2$ (0.22 M) in dimethylformamide:DMSO 4:1 v:v. An 88.9 µL aliquot of solution 1 was transferred into solution 2 and then spin-coated by two following steps: 1) 1000 rpm (acceleration rate 5000 rpm s^{-1}) for 10 s, 2) 6000 rpm (acceleration rate 5000 rpm s^{-1}) for 20 s. 6–7 s before the end of second step 100 µL chlorobenzene (Sigma Aldrich), as anti-solvent, was released on the spinning substrate. The samples were annealed at 100 °C for 1 h in nitrogen atmosphere. As buffer layer, undoped poly[bis(4-phenyl)(2,4,6-trimethylphenyl)amine] (PTAA, EMindex Co. Ltd.) was used which was deposited in a solution-based approach. For this, PTAA was dissolved in anhydrous toluene (99.8%, Sigma Aldrich) with a concentration of 0.8 mg mL^{-1} and spin-coated for 30 s at a rotation speed of 5000 rpm in a nitrogen-filled glovebox. Directly after the spin-coating, the samples were annealed at 100 °C for 10 min.

For the opaque devices, a 100 µm thick PEN foil (TEONEX Q65HA) was used (also 16 mm × 16 mm). The PEN foil was cleaned analog to the other substrates. An 80 nm thick gold electrode was evaporated using a thermal evaporator (Vactec Coat 320). Subsequently 20 nm thick NiO_x HTLs were sputtered using a Pro Line PVD75 (Kurt J. Lesker Company) at 1 mTorr process pressure at 100 W under rf-conditions in combination with a NiO target (Kurt J. Lesker Company, 99.995% metallic purity). Argon was used as process gas. The base pressure in the chamber was $<1 \times 10^{-7}$ mTorr.

Hot Pressing: The lamination of perovskite solar cells was performed with a vacuum hot embossing machine developed in-house in cooperation with Jenoptik Mikrotechnik (details are reported in ref. [72] in chapter 2.5.1). The embossing machine was consisted of an upper fixed crossbar and the lower crossbar movable by a spindle drive. The lower and upper plates were heated and cooled via an oil heating and cooling unit. The operation pressure for samples up to 4 in. wafers, was ranged from 0 to 200 kN and the maximum temperature was 190 °C. The sample chamber was connected to a vacuum pump. For the lamination of the upper and lower half of the layer stack of the perovskite solar cell, both parts were placed on top of each other in between the planar plates. To distribute the pressure more homogenously, the stacked parts were placed between two sheets of aluminum foils (thickness 200 µm) on each side. A silicon wafer was placed on the foil side, but with the two aluminum sheets between itself and the foil. The lamination of the perovskite solar cells was performed at 50 ± 10 MPa.

Characterization: The characterization of the laminated perovskite solar cells was performed inside a glovebox with a controlled nitrogen atmosphere (oxygen level < 10 ppm, water level < 1 ppm). The solar cell current density–voltage characteristics were measured with a xenon-lamp-based solar simulator (Newport Oriel Sol3A) in both forward and backward direction (scan rate 0.6 V s^{-1}). The intensity was calibrated with a KG5-filtered silicon reference solar cell to match the global standard spectrum with air mass 1.5 (AM1.5 G) with an intensity of 100 mW cm^{-2}. The short-circuit current density of the *J–V* measurement was scaled to the calculated J_{SC} of the external quantum efficiency measurement (see Figure 2b) to eliminate uncertainties in the exact active surface area (≈10.5 mm^2). The standard measurements were performed at 25 °C using a microcontroller in combination with a Peltier-element to control the sample temperature. The same holder was used to heat and cool the samples for the reported measurements with varying temperatures. Due to the limitations of the sample holder, the maximum temperature at which the perovskite cells could be measured was limited to 80 °C. The external quantum efficiency (EQE) was measured using a dedicated system (Bentham PVE300 EQE). A chopping frequency of 820 Hz with an integration time of 500 ms was used to obtain the spectra. Reflectance and transmittance measurements were performed with a spectrophotometer (PerkinElmer Lambda 1050). For the measurement of the *J–V* characteristics, the EQE, and the reflectance, the laminated perovskite solar cells were not additionally encapsulated. The surface profile was measured with an AFM (NanoWizard II from JPK Instruments AG, Germany). The crystal structure was examined using XRD (Bruker D2 PHASER) using Cu Kα radiation.

Supporting Information

Supporting Information is available from the Wiley Online Library or from the author.

Acknowledgements

R.S. and J.R. contributed equally to this work. The authors thank I. M. Hossain for fruitful discussions and N. Rai, H. Hu, R. Pokratath, and M. Schneider for their experimental assistance. The authors also gratefully acknowledge the financial support by the Helmholtz Association through the program "Science and Technology of Nanosystems" (STN),

the HYIG of U.W. Paetzold (FKZ VH-NG-1148), the project PEROSEED (FKZ ZT-0024), the Helmholtz Energy Materials Foundry (HEMF), and the Recruitment Initiative of B.S. Richards. The research was support by the Karlsruhe School of Optics & Photonics (KSOP).

Conflict of Interest

The authors declare no conflict of interest.

Keywords

lamination, perovskite interfaces, perovskite solar cells, thermal stability

Received: September 10, 2019
Revised: December 6, 2019
Published online: January 9, 2020

[1] National Renewable Energy Laboratory (NREL), *Solar Cell Efficiency Chart*, https://www.nrel.gov/pv/assets/pdfs/best-research-cell-efficiencies.20191106.pdf (accessed: December 2019).
[2] S. D. Stranks, G. E. Eperon, G. Grancini, C. Menelaou, M. J. P. Alcocer, T. Leijtens, L. M. Herz, A. Petrozza, H. J. Snaith, *Science* **2013**, *342*, 341.
[3] L. M. Pazos-Outón, M. Szumilo, R. Lamboll, J. M. Richter, M. Crespo-Quesada, M. Abdi-Jalebi, H. J. Beeson, M. Vrućinić, M. Alsari, H. J. Snaith, B. Ehrler, R. H. Friend, F. Deschler, *Science* **2016**, *351*, 1430.
[4] M. Saliba, J. P. Correa-Baena, M. Grätzel, A. Hagfeldt, A. Abate, *Angew. Chem., Int. Ed.* **2018**, *57*, 2554.
[5] I. A. Howard, T. Abzieher, I. M. Hossain, H. Eggers, F. Schackmar, S. Ternes, B. S. Richards, U. Lemmer, U. W. Paetzold, *Adv. Mater.* **2019**, *31*, 1806702.
[6] B. R. Sutherland, E. H. Sargent, *Nat. Photonics* **2016**, *10*, 295.
[7] M. H. Futscher, B. Ehrler, *ACS Energy Lett.* **2016**, *1*, 863.
[8] G. E. Eperon, M. T. Hörantner, H. J. Snaith, *Nat. Rev. Chem.* **2017**, *1*, 0095.
[9] M. Saliba, T. Matsui, K. Domanski, J. Y. Seo, A. Ummadisingu, S. M. Zakeeruddin, J. P. Correa-Baena, W. R. Tress, A. Abate, A. Hagfeldt, M. Grätzel, *Science* **2016**, *354*, 206.
[10] H. Tsai, W. Nie, J. C. Blancon, C. C. Stoumpos, R. Asadpour, B. Harutyunyan, A. J. Neukirch, R. Verduzco, J. J. Crochet, S. Tretiak, L. Pedesseau, J. Even, M. A. Alam, G. Gupta, J. Lou, P. M. Ajayan, M. J. Bedzyk, M. G. Kanatzidis, A. D. Mohite, *Nature* **2016**, *536*, 312.
[11] M. Saliba, J. P. Correa-Baena, C. M. Wolff, M. Stolterfoht, N. Phung, S. Albrecht, D. Neher, A. Abate, *Chem. Mater.* **2018**, *30*, 4193.
[12] E. H. Jung, N. J. Jeon, E. Y. Park, C. S. Moon, T. J. Shin, T. Y. Yang, J. H. Noh, J. Seo, *Nature* **2019**, *567*, 511.
[13] J. Peng, J. I. Khan, W. Liu, E. Ugur, T. Duong, Y. Wu, H. Shen, K. Wang, H. Dang, E. Aydin, X. Yang, Y. Wan, K. J. Weber, K. R. Catchpole, F. Laquai, S. De Wolf, T. P. White, *Adv. Energy Mater.* **2018**, *8*, 1801208.
[14] S. Gharibzadeh, B. Abdollahi Nejand, M. Jakoby, T. Abzieher, D. Hauschild, S. Moghadamzadeh, J. A. Schwenzer, P. Brenner, R. Schmager, A. A. Haghighirad, L. Weinhardt, U. Lemmer, B. S. Richards, I. A. Howard, U. W. Paetzold, *Adv. Energy Mater.* **2019**, *9*, 1803699.
[15] T. Abzieher, S. Moghadamzadeh, F. Schackmar, H. Eggers, F. Sutterlüti, A. Farooq, D. Kojda, K. Habicht, R. Schmager, A. Mertens, R. Azmi, L. Klohr, J. A. Schwenzer, M. Hetterich, U. Lemmer, B. S. Richards, M. Powalla, U. W. Paetzold, *Adv. Energy Mater.* **2019**, *9*, 1802995.
[16] Q. Jiang, X. Zhang, J. You, *Small* **2018**, *14*, 1801154.
[17] T. Abzieher, J. A. Schwenzer, F. Sutterlüti, M. Pfau, E. Lotter, M. Hetterich, U. Lemmer, M. Powalla, U. W. Paetzold, in *2018 IEEE 7th World Conf. Photovoltaic Energy Conversion*, IEEE, Piscataway, NJ **2018**, pp. 2803–2807.
[18] S. Sajid, A. M. Elseman, H. Huang, J. Ji, S. Dou, H. Jiang, X. Liu, D. Wei, P. Cui, M. Li, *Nano Energy* **2018**, *51*, 408.
[19] N. Arora, M. I. Dar, A. Hinderhofer, N. Pellet, F. Schreiber, S. M. Zakeeruddin, M. Grätzel, *Science* **2017**, *358*, 768.
[20] Y.-F. Li, *J. Phys. Chem. C* **2019**, *123*, 14164.
[21] E. H. Anaraki, A. Kermanpur, L. Steier, K. Domanski, T. Matsui, W. Tress, M. Saliba, A. Abate, M. Grätzel, A. Hagfeldt, J. P. Correa-Baena, *Energy Environ. Sci.* **2016**, *9*, 3128.
[22] Q. Dong, J. Li, Y. Shi, M. Chen, L. K. Ono, K. Zhou, C. Zhang, Y. Qi, Y. Zhou, N. P. Padture, L. Wang, *Adv. Energy Mater.* **2019**, *9*, 1900834.
[23] J. Y. Seo, R. Uchida, H. S. Kim, Y. Saygili, J. Luo, C. Moore, J. Kerrod, A. Wagstaff, M. Eklund, R. McIntyre, N. Pellet, S. M. Zakeeruddin, A. Hagfeldt, M. Grätzel, *Adv. Funct. Mater.* **2018**, *28*, 1705763.
[24] I. M. Hossain, D. Hudry, F. Mathies, T. Abzieher, S. Moghadamzadeh, D. Rueda-Delgado, F. Schackmar, M. Bruns, R. Andriessen, T. Aernouts, F. Di Giacomo, U. Lemmer, B. S. Richards, U. W. Paetzold, A. Hadipour, *ACS Appl. Energy Mater.* **2019**, *2*, 47.
[25] D. A. Jacobs, M. Langenhorst, F. Sahli, B. S. Richards, T. P. White, C. Ballif, K. R. Catchpole, U. W. Paetzold, *J. Phys. Chem. Lett.* **2019**, *10*, 3159.
[26] T. Li, W. A. Dunlap-Shohl, Q. Han, D. B. Mitzi, *Chem. Mater.* **2017**, *29*, 6200.
[27] B. Abdollahi Nejand, V. Ahmadi, H. R. Shahverdi, *ACS Appl. Mater. Interfaces* **2015**, *7*, 21807.
[28] K. A. Bush, A. F. Palmstrom, Z. J. Yu, M. Boccard, R. Cheacharoen, J. P. Mailoa, D. P. McMeekin, R. L. Z. Hoye, C. D. Bailie, T. Leijtens, I. M. Peters, M. C. Minichetti, N. Rolston, R. Prasanna, S. Sofia, D. Harwood, W. Ma, F. Moghadam, H. J. Snaith, T. Buonassisi, Z. C. Holman, S. F. Bent, M. D. McGehee, *Nat. Energy* **2017**, *2*, 17009.
[29] E. Nouri, Y. L. Wang, Q. Chen, J. J. Xu, G. Paterakis, V. Dracopoulos, Z. X. Xu, D. Tasis, M. R. Mohammadi, P. Lianos, *Electrochim. Acta* **2017**, *233*, 36.
[30] S. Guarnera, A. Abate, W. Zhang, J. M. Foster, G. Richardson, A. Petrozza, H. J. Snaith, *J. Phys. Chem. Lett.* **2015**, *6*, 432.
[31] F. Sahli, J. Werner, B. A. Kamino, M. Bräuninger, R. Monnard, B. Paviet-Salomon, L. Barraud, L. Ding, J. J. Diaz Leon, D. Sacchetto, G. Cattaneo, M. Despeisse, M. Boccard, S. Nicolay, Q. Jeangros, B. Niesen, C. Ballif, *Nat. Mater.* **2018**, *17*, 820.
[32] Z. Li, S. A. Kulkarni, P. P. Boix, E. Shi, A. Cao, K. Fu, S. K. Batabyal, J. Zhang, Q. Xiong, L. H. Wong, N. Mathews, S. G. Mhaisalkar, *ACS Nano* **2014**, *8*, 6797.
[33] P. You, Z. Liu, Q. Tai, S. Liu, F. Yan, *Adv. Mater.* **2015**, *27*, 3632.
[34] J. H. Heo, D. H. Shin, M. L. Lee, M. G. Kang, S. H. Im, *ACS Appl. Mater. Interfaces* **2018**, *10*, 31413.
[35] M. Makha, S. L. Fernandes, S. Jenatsch, T. Offermans, J. Schleuniger, J. N. Tisserant, A. C. Véron, R. Hany, *Sci. Technol. Adv. Mater.* **2016**, *17*, 260.
[36] J. H. Heo, S. H. Im, *Adv. Mater.* **2016**, *28*, 5121.
[37] C. O. Ramírez Quiroz, G. D. Spyropoulos, M. Salvador, L. M. Roch, M. Berlinghof, J. Darío Perea, K. Forberich, L. Dion-Bertrand, N. J. Schrenker, A. Classen, N. Gasparini, G. Chistiakova, M. Mews, L. Korte, B. Rech, N. Li, F. Hauke, E. Spiecker, T. Ameri, S. Albrecht, G. Abellán, S. León, T. Unruh, A. Hirsch, A. Aspuru-Guzik, C. J. Brabec, *Adv. Funct. Mater.* **2019**, *29*, 1901476.
[38] C. W. Jang, J. M. Kim, S.-H. Choi, *J. Alloys Compd.* **2019**, *775*, 905.

[39] H. Zhang, Y. Zhang, G. Yang, Z. Ren, W. Yu, D. Shen, C.-S. Lee, Z. Zheng, G. Li, *Sci. China Chem.* **2019**, *62*, 875.
[40] Y. Shao, C. Zhang, S. Wang, Y. Yan, Y. Feng, J. Bian, Y. Shi, *Adv. Mater. Interfaces* **2019**, *6*, 1900157.
[41] W. A. Dunlap-Shohl, T. Li, D. B. Mitzi, *ACS Appl. Energy Mater.* **2019**, *2*, 5083.
[42] F. Jiang, T. Liu, S. Zeng, Q. Zhao, X. Min, Z. Li, J. Tong, W. Meng, S. Xiong, Y. Zhou, *Opt. Express* **2015**, *23*, A83.
[43] S. P. Dunfield, D. T. Moore, T. R. Klein, D. M. Fabian, J. A. Christians, A. G. Dixon, B. Dou, S. Ardo, M. C. Beard, S. E. Shaheen, J. J. Berry, M. F. A. M. Van Hest, *ACS Energy Lett.* **2018**, *3*, 1192.
[44] L. Shi, M. Zhang, Y. Cho, T. L. Young, D. Wang, H. Yi, J. Kim, S. Huang, A. W. Y. Ho-Baillie, *ACS Appl. Energy Mater.* **2019**, *2*, 2358.
[45] W. W. Kim, M. S. Jung, S. Lee, Y. J. Choi, J. K. Kim, S. U. Chai, W. W. Kim, D. D. G. Choi, H. Ahn, J. H. Cho, D. D. G. Choi, H. Shin, D. Kim, J. H. Park, *Adv. Energy Mater.* **2018**, *8*, 1702369.
[46] A. K. Jena, Y. Numata, M. Ikegami, T. Miyasaka, *J. Mater. Chem. A* **2018**, *6*, 2219.
[47] K. Domanski, E. A. Alharbi, A. Hagfeldt, M. Grätzel, W. Tress, *Nat. Energy* **2018**, *3*, 61.
[48] J. Cao, H. Yu, S. Zhou, M. Qin, T. K. Lau, X. Lu, N. Zhao, C. P. Wong, *J. Mater. Chem. A* **2017**, *5*, 11071.
[49] J. A. Schwenzer, L. Rakocevic, R. Gehlhaar, T. Abzieher, S. Gharibzadeh, S. Moghadamzadeh, A. Quintilla, B. S. Richards, U. Lemmer, U. W. Paetzold, *ACS Appl. Mater. Interfaces* **2018**, *10*, 16390.
[50] T. Abzieher, J. A. Schwenzer, S. Moghadamzadeh, F. Sutterluti, I. M. Hossain, M. Pfau, E. Lotter, M. Hetterich, B. S. Richards, U. Lemmer, M. Powalla, U. W. Paetzold, *IEEE J. Photovoltaics* **2019**, *9*, 1249.
[51] S. Mashhoun, Y. Hou, H. Chen, F. Tajabadi, N. Taghavinia, H. J. Egelhaaf, C. J. Brabec, *Adv. Energy Mater.* **2018**, *8*, 1802085.
[52] Y. Guo, J. Tao, J. Jiang, J. Zhang, J. Yang, S. Chen, J. Chu, *Sol. Energy Mater. Sol. Cells* **2018**, *188*, 66.
[53] K. Domanski, B. Roose, T. Matsui, M. Saliba, S. H. Turren-Cruz, J. P. Correa-Baena, C. R. Carmona, G. Richardson, J. M. Foster, F. De Angelis, J. M. Ball, A. Petrozza, N. Mine, M. K. Nazeeruddin, W. Tress, M. Grätzel, U. Steiner, A. Hagfeldt, A. Abate, *Energy Environ. Sci.* **2017**, *10*, 604.
[54] M. Saliba, M. Stolterfoht, C. M. Wolff, D. Neher, A. Abate, *Joule* **2018**, *2*, 1019.
[55] C. Zhang, S. Wang, H. Zhang, Y. Feng, W. Tian, Y. Yan, J. Bian, Y. Wang, S. Jin, S. M. Zakeeruddin, M. Grätzel, Y. Shi, *Energy Environ. Sci.* **2019**, *12*, 3585.
[56] N. Arora, M. I. Dar, S. Akin, R. Uchida, T. Baumeler, Y. Liu, S. M. Zakeeruddin, M. Grätzel, *Small* **2019**, *15*, 1904746.
[57] S. H. Turren-Cruz, A. Hagfeldt, M. Saliba, *Science* **2018**, *362*, 449.
[58] E. A. Alharbi, A. Y. Alyamani, D. J. Kubicki, A. R. Uhl, B. J. Walder, A. Q. Alanazi, J. Luo, A. Burgos-Caminal, A. Albadri, H. Albrithen, M. H. Alotaibi, J.-E. Moser, S. M. Zakeeruddin, F. Giordano, L. Emsley, M. Grätzel, *Nat. Commun.* **2019**, *10*, 3008.
[59] R. Cheacharoen, C. C. Boyd, G. F. Burkhard, T. Leijtens, J. A. Raiford, K. A. Bush, S. F. Bent, M. D. McGehee, *Sustainable Energy Fuels* **2018**, *2*, 2398.
[60] S. Barard, M. Heeney, L. Chen, M. Cölle, M. Shkunov, I. Mcculloch, N. Stingelin, M. Philips, T. Kreouzis, *J. Appl. Phys.* **2009**, *105*, 013701.
[61] A. Mayer, M. Buchmüller, S. Wang, C. Steinberg, M. Papenheim, H.-C. Scheer, N. Pourdavoud, T. Haeger, T. Riedl, *J. Vac. Sci. Technol., B: Nanotechnol. Microelectron.: Mater., Process., Meas., Phenom.* **2017**, *35*, 06G803.
[62] N. Pourdavoud, S. Wang, A. Mayer, T. Hu, Y. Chen, A. Marianovich, W. Kowalsky, R. Heiderhoff, H.-C. Scheer, T. Riedl, *Adv. Mater.* **2017**, *29*, 1605003.
[63] R. Schmager, T. Abzieher, P. Brenner, A. Assadillayev, D. J. Lee, S. Moghadamzadeh, I. M. Hossain, U. Lemmer, B. S. Richards, U. W. Paetzold, in *2018 IEEE 7th World Conf. Photovoltaic Energy Conversion*, IEEE, Piscataway, NJ **2018**, pp. 15–17.
[64] N. Pourdavoud, A. Mayer, M. Buchmüller, K. Brinkmann, T. Häger, T. Hu, R. Heiderhoff, I. Shutsko, P. Görrn, Y. Chen, H. C. Scheer, T. Riedl, *Adv. Mater. Technol.* **2018**, *3*, 1700253.
[65] R. Schmager, G. Gomard, B. S. Richards, U. W. Paetzold, *Sol. Energy Mater. Sol. Cells* **2019**, *192*, 65.
[66] M. Saliba, T. Matsui, J. Y. Seo, K. Domanski, J. P. Correa-Baena, M. K. Nazeeruddin, S. M. Zakeeruddin, W. Tress, A. Abate, A. Hagfeldt, M. Grätzel, *Energy Environ. Sci.* **2016**, *9*, 1989.
[67] W. Zhou, S. Chen, Y. Zhao, Q. Li, Y. Zhao, R. Fu, D. Yu, P. Gao, Q. Zhao, *Adv. Funct. Mater.* **2019**, *29*, 1809180.
[68] H. B. Lee, M. K. Jeon, N. Kumar, B. Tyagi, J. W. Kang, *Adv. Funct. Mater.* **2019**, *29*, 1903213.
[69] A. Farooq, I. M. Hossain, S. Moghadamzadeh, J. A. Schwenzer, T. Abzieher, B. S. Richards, E. Klampaftis, U. W. Paetzold, *ACS Appl. Mater. Interfaces* **2018**, *10*, 21985.
[70] Y. Wang, T. Li, Z. Li, S. Wang, X. Deng, *Adv. Funct. Mater.* **2019**, *29*, 1903330.
[71] P. Cui, D. Wei, J. Ji, H. Huang, E. Jia, S. Dou, T. Wang, W. Wang, M. Li, *Nat. Energy* **2019**, *4*, 150.
[72] M. Worgull, *Hot Embossing: Theory and Technology of Microreplication*, Elsevier, New York **2009**.